JPE 14-3-4

http://dx.doi.org/10.6113/JPE.2014.14.3.444
ISSN(Print): 1598-2092 / ISSN(Online): 2093-4718

Design and Realization of a Digital PV Simulator with a Push-Pull Forward Circuit

Jike Zhang†, Shengtie Wang*, Zhihe Wang*, and Lixin Tian*

†*College of Electric Power, Inner Mongolia University of Technology, Hohhot, China

Abstract

This paper presents the design and realization of a digital PV simulator with a Push-Pull Forward (PPF) circuit based on the principle of modular hardware and configurable software. A PPF circuit is chosen as the main circuit to restrain the magnetic biasing of the core for a DC-DC converter and to reduce the spike of the turn-off voltage across every switch. Control and I/O interface based on a personal computer (PC) and multifunction data acquisition card, can conveniently achieve the data acquisition and configuration of the control algorithm and interface due to the abundant software resources of computers. In addition, the control program developed in Matlab/Simulink can conveniently construct and adjust both the models and parameters. It can also run in real-time under the external mode of Simulink by loading the modules of the Real-Time Windows Target. The mathematic models of the Push-Pull Forward circuit and the digital PV simulator are established in this paper by the state-space averaging method. The pole-zero cancellation technique is employed and then its controller parameters are systematically designed based on the performance analysis of the root loci of the closed current loop with k_i and R_L as variables. A fuzzy PI controller based on the Takagi-Sugeno fuzzy model is applied to regulate the controller parameters self-adaptively according to the change of R_L and the operating point of the PV simulator to match the controller parameters with R_L. The stationary and dynamic performances of the PV simulator are tested by experiments, and the experimental results show that the PV simulator has the merits of a wide effective working range, high steady-state accuracy and good dynamic performances.

Key words: Digital PV simulator, Fuzzy PI controller, Push-Pull Forward circuit, Pole-zero cancellation, Root locus method, State-space averaging method

I. INTRODUCTION

In recent years, due to the serious problems of energy shortages, environmental pollution and energy security throughout the world, the development and utilization of clean renewable energy is becoming an important way to improve the energy structure, reduce environment pollution and persistently ensure the energy supply all over the world [1], [2]. The worldwide interest in renewable energy has greatly promoted the development of PV generation technology and industry [3]-[5].

In the research and development of PV generation systems, if a real PV array is used to test and verify the correctness and performance of the power electronic equipment and control systems, it would be both costly and time-consuming. Therefore, the output characteristics of a PV array under various operating conditions are always simulated by a PV simulator, which can be made by an analog circuit, a digital circuit or an analog and digital hybrid circuit. There are several methods to implement a PV simulator, including:

1) amplifying the output of the current and voltage of a sample PV cell or photosensor diode with a controlled light source imitating sunlight or an LED light emission circuit to simulate variations in sunshine intensity [6], [7]
2) constructing a PV array by taking a PV cell equivalent circuit with analog circuits as a basic unit [8]
3) using a DC power supply controlled by a personal computer (PC) with a data acquisition card or a special real time digital simulator (such as RT-LAB) [9], [10]
4) adopting a unidirectional DC-DC converter with a basic topology controlled by a DSP, a PC, a microprocessor, a microcontroller, or some other

Manuscript received Oct. 6, 2013; revised Feb. 4, 2014
Recommended for publication by Associate Editor Joung-Hu Park.
†Corresponding Author: zhangjike@imut.edu.cn
Tel: +86-471-657-6044, Fax: +86-471-360-2300, Inner Mongolia Univ. of Tech.
*College of Electric Power, Inner Mongolia Univ. of Technology, China

TABLE I
CHARACTERISTICS COMPARISON OF DIFFERENT METHODS FOR PV SIMULATOR

	Method 1	Method 2	Method 3	Method 4	Method 5	Method 6	Method 7	The proposed method
Topology	DC power amplifier	PV module equivalent analog circuit	Controllable DC power supply	DC power supply(or uncontrolled diode rectifier)+unidirectional DC/DC converter	PWM rectifier+ bidirectional compound DC/DC converter	multiple multiphase DC/DC converter	High frequency PWM rectifier of three-phase voltage source	DC power supply +Push-Pull Forward converter
Electrical isolation	NO	NO	—	NO	NO	YES	NO	YES
Core magnetic biasing restraint	—	—	—	—	—	—	—	YES
I-V characteristics realized by	Sample PV cell or photo diode	Industry PC	PC or real time digital simulator	DSP, PC, microprocessor, or microcontroller	DSP	PC or DSP	Host computer	PC
Development software	—	—	MATLAB /Simulink, Labview	Assembly language or high level language	Assembly language or high level language	Labview or other software	—	MATLAB /Simulink
Modeling and controller design method	—	—	—	NO	—	—	NO	YES
Effective working range	Wider	Wide	Wide	Wide	Wide	Wide	Wide	Wide
Accuracy	Poor	High	High	High	High	High	Higher	Higher
System development efficiency	Low	Low	High	High	High	High	High	Higher

digital control technology as the main circuit of the digital PV simulator to simulate the output characteristics of the PV array, where the DC input voltage is supplied by a DC power supply or an uncontrolled diode rectifier [11]-[14]

5) adopting the topology of a PWM rectifier with a bidirectional compound DC/DC converter controlled by a DSP or a PC [15]
6) using multiple multiphase DC/DC converters controlled by a PC or a DSP as the main circuit of the PV simulator [16], [17]
7) selecting a high frequency PWM rectifier for a three-phase voltage source controlled by the host computer as the main circuit of the PV simulator [18].

Despite achieving adequate simulative effects, most of the PV simulators still exhibit some problems, such as a limited effective working range, bigger ripples of the output voltage and current, lack of systematic modeling and design methods for the controller parameters, lower development efficiency, and so on.

Considering the above drawbacks, the digital PV simulator presented in this paper adopts modular hardware, configurable software, systematic modeling and design methods for the controller parameters so as to obtain the merits of a wide effective working range, high steady-state accuracy, good control performances, high reliability and development efficiency. A comparison of the characteristics of the different methods for PV simulators is listed in Table I.

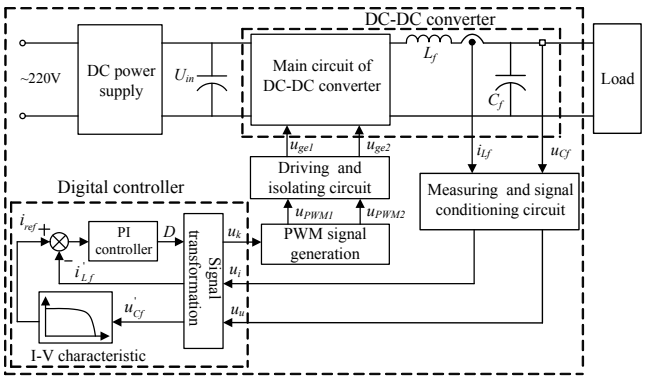

Fig. 1. Overall configuration of the digital PV simulator.

II. CONFIGURATION AND WORKING PRINCIPLE OF THE DIGITAL PV SIMULATOR

The overall configuration of the digital PV simulator is shown in Fig. 1. It mainly consists of a DC power supply, a DC-DC converter, a digital controller, a PWM signal generation circuit, a measuring and signal conditioning circuit, a driving and isolating circuit, and so on. The main operation

principle is as follows: the DC power supply provides a steady DC input voltage for the DC-DC converter. According to the output voltage measured in real-time, the digital controller calculates the reference current signal by the I-V characteristic model and then calculates the duty ratio of the converters' PWM signals by a current closed-loop regulator. After signal conversion, the duty ratio is converted into a signal-level control voltage which is sent to the PWM signal generation circuit to generate PWM signals. The PWM signals control the states of the power switches so as to adjust the converter's output voltage and current after signal isolation and power driving. Finally, the PV simulator can always work at a certain operational point at which the output voltage and output current of the converter can satisfy both the load characteristics and the I-V curve of the PV array. Thus, the output characteristics of the PV array can be easily simulated by the digital PV simulator.

III. WORKING MECHANISM OF THE PUSH-PULL FORWARD CIRCUIT

A. Circuit Structure

The main circuit of the DC-DC converter adopts a Push-Pull Forward (PPF) circuit in the PV simulator. A full-wave rectifier is applied in the secondary windings of the high frequency transformer so as to reduce the conduction losses of the rectifying diodes with a low-output voltage and a high-output current. An LC filter is used to provide a continuous load current and to reduce harmonics. Fig. 2 shows the topological structure of the DC-DC converter. It can be seen from the figure that the PPF circuit is different from a conventional Push-Pull converter in that a clamping capacitor is connected in series between the two primary windings of the high frequency transformer and between the two power switches. As a result, it has the advantages of both the Push-Pull converter and Forward converter, and it can restrain the magnetic biasing of the core for the DC-DC converter, magnetize the magnetic core bi-directionally and reduce the spike in the turn-off voltage across each switch. Therefore, the PPF circuit is becoming a kind of preponderant circuit topology for low voltage and high current output applications.

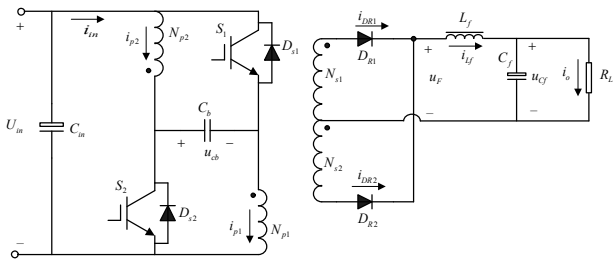

Fig. 2. Diagram of Push-Pull Forward circuit.

B. Analysis of the Operating Modes

In steady state, the PPF circuit has 8 operating modes in a switch cycle. Each power switch matches with the 4 operating modes of one cycle. In the following analysis, it is assumed that all of the power switches and diodes are ideal components and that the on-state voltage drops for all of the power electronic components are negligible [19]. The equivalent circuits of the former four operating modes are shown in Fig.3.

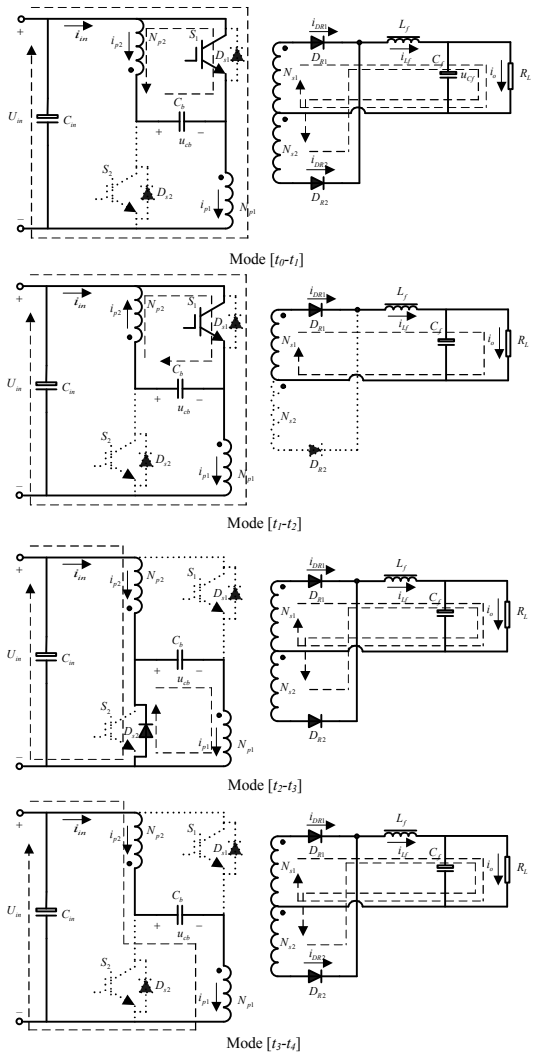

Fig. 3. Equivalent circuits of the former four operating modes in a switch cycle.

1) Mode [t_0-t_1]: Prior to t_0, the power switches S_1 and S_2 are off. The primary current freewheels through $U_{in(+)}\rightarrow N_{p2}\rightarrow C_b\rightarrow N_{p1}\rightarrow U_{in(-)}$ and forms a circular current which is $I_a=i_{p1}=i_{p2}$. During this period, the rectifying diodes of the secondary windings turn on simultaneously, and the current through each of the rectifying diodes is $i_{DR1}= i_{DR2}=I_o/2$. At t_0, the filtering inductor current runs down to the minimum value I_{Lfmin} .

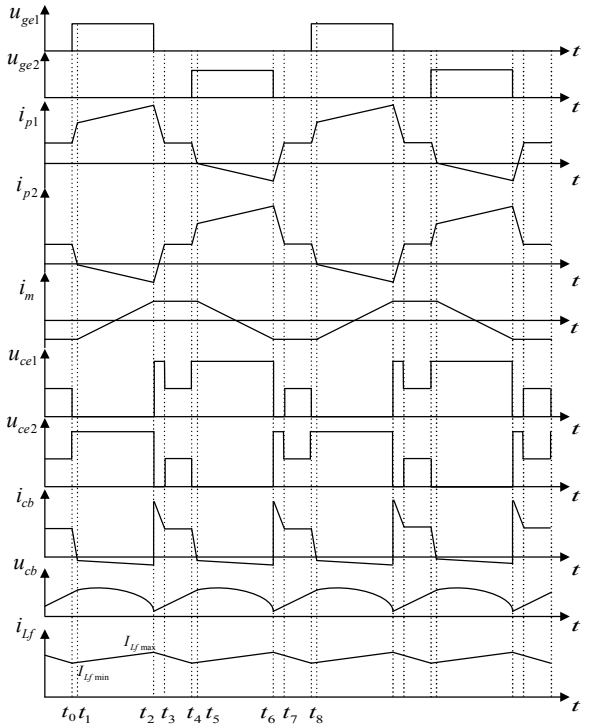

Fig. 4. Key waveforms of Push-Pull Forward circuit.

At t_0, S_1 turns on. U_{in} and u_{cb} are applied to the leakage inductances L_σ of N_{p1} and N_{p2}, respectively. i_{p1} increases rapidly due to U_{in} being in the same direction as i_{p1}, and i_{p2} decreases rapidly due to u_{cb} being in the opposite direction as i_{p2}. Corresponding with i_{p1} and i_{p2}, i_{DR1} and i_{DR2} increase and decreases respectively because of the affection of the magnetic circuit. During this period, the filtering inductor current increases gradually from I_{Lfmin}. This mode ends when i_{DR1} is equal to the load current, both i_{p2} and i_{DR2} are decreased to 0 and the commutation process ends. The voltage across S_1 is always $2U_{in}$ during this period.

2) Mode $[t_1$-$t_2]$: In this mode, U_{in} and u_{cb} are applied to the magnetizing inductor L_m and the primary reduced inductance of the filtering inductances L_f of N_{p1} and N_{p2}, respectively. Each half of the changing rate of the magnetizing current and load current is shared by the primary winding. i_{p1} continues to increase in the original direction defined as the reference direction whereas i_{p2} increases gradually from 0 in the opposite direction. This mode lasts from t_1 to t_2 and S_1 turns off at t_2. Because the circuit works like two forward converters in parallel, the circuit is called Push-Pull Forward circuit or converter. At the instant of S_1 turning off, i_{p1} runs up to the maximum value, because both the magnetizing current and primary reduced current of the load current flow through S_1. The filtering inductor current also runs up to the maximum value accordingly. The voltage across S_1 is also $2U_{in}$ during this period.

3) Mode $[t_2$-$t_3]$: After S_1 turns off, the body diode D_{S2} of S_2 is forced to turn on to continue the leakage inductance current because i_{p1} is always larger than i_{p2} before t_2. The energy of the leakage inductance is released to charge the clamping capacitor C_b through the low impedance loop $N_{p1}\rightarrow D_{S2}\rightarrow C_b$. U_{in} and u_{cb} are applied to the leakage inductances of N_{p2} and N_{p1}, respectively. i_{p1} decreases rapidly, and i_{p2} reduces to 0 gradually and then changes direction to increase rapidly in the reference direction. i_{DR1} and i_{DR2} decrease and increase, respectively. When i_{DR1} and i_{DR2} reach the same value I_a at t_3, this mode ends. During this period, the load current decreases gradually from I_{Lfmax}.

4) Mode $[t_3$-$t_4]$: During this period, both S_1 and S_2 are off, and the leakage inductance current is freewheeling through $U_{in(+)}\rightarrow N_{p2}\rightarrow C_b\rightarrow N_{p1}\rightarrow U_{in(-)}$ and forms a circular current in the primary windings. Due to the two primary windings being series-opposing connections, the voltages across them are both 0 and the voltages across the power switches are both U_{in}. At the same time, magnetizing current also forms a circular current in the secondary side of the high frequency transformer. This mode ends when S_2 turns on at t_4.

5) Mode $[t_4$-$t_5][t_5$-$t_6][t_6$-$t_7][t_7$-$t_8]$: At t_4, S_2 turns on and the circuit goes into the second half of a switch cycle. The modes $[t_4$-$t_5]$, $[t_5$-$t_6]$, $[t_6$-$t_7]$ and $[t_7$-$t_8]$ in the second half of a switch cycle correspond to $[t_0$-$t_1]$, $[t_1$-$t_2]$, $[t_2$-$t_3]$ and $[t_3$-$t_4]$, respectively. The operating principle of the second half of a switch cycle works in the same way as the first half, except that the magnetizing currents of the two half cycles are opposite in direction. During the second half of a switch cycle, demagnetization of the high frequency transformer is completed.

The key operating waveforms are shown in Fig.4.

C. Input-Output Relationship

Suppose the primary winding turn of the transformer is N_{P1}=N_{P2}=w_1 and its secondary winding turn is N_{s1}=N_{s2}=w_2, then the turns ratio of the secondary to primary is n=w_2/w_1. The duty ratio D is defined as $2T_{on}/T_s$, where T_{on} is the on duration of each power switch (S_1 or S_2) and T_s is the switch time period which is equal to the reciprocal of the switching frequency f_s.

During steady-state operation, the filtering inductor current is of the triangle waveform, and it varies periodically between I_{Lfmin} and I_{Lfmax}. The inductor current increase $\Delta I_{Lf(+)}$, during the on duration of S_1 or S_2, is equal to its decrease $\Delta I_{Lf(-)}$ while S_1 and S_2 are both off. The relationship between them can be expressed as:

$$\Delta I_{Lf(+)} = \Delta I_{Lf(-)} = \Delta I_{Lf} = \frac{U_o}{L_f}\cdot\frac{(1-D)T_s}{2} \qquad (1)$$

Thus:

$$\frac{nU_{in}-U_o}{L_f}\cdot\frac{DT_s}{2}=\frac{U_o}{L_f}\cdot\frac{(1-D)T_s}{2} \tag{2}$$

That is:

$$U_o=nDU_{in} \tag{3}$$

where U_{in} and U_o are the average input voltage and output voltage, respectively.

If the power losses of the circuit are neglected, the average input current can be expressed as :

$$I_{in}=nDI_o \tag{4}$$

where I_o is the average load current, $I_o=(I_{Lfmin}+I_{Lfmax})/2$.

IV. Modeling of the Digital PV Simulator

Fig. 5 shows a control block diagram of the digital PV simulator. There are two control loops in it: the outer-reference loop and the inner-current loop. The former measures the output voltage u_o of the PV simulator and feeds it back to the I-V characteristic mode so as to generate the reference current i_{ref}; while the latter controls the filtering inductor current i_{Lf}. R_L represents the equivalent load resistance of the PV simulator's load characteristics; $G(s)$ is the transfer function of the duty ratio to the filtering inductor current; $G_c(s)$ is the transfer function of the PI controller, $G_c(s)=k_p+k_i/s$; $G_{fi}(s)$ is the equivalent transfer function of the current measuring, conditioning and filtering, $G_{fi}(s)=1/(T_{f1}s+1)$; and $G_{fu}(s)$ is the equivalent transfer function of the voltage measuring, conditioning and filtering, $G_{fu}(s)=1/(T_{f2}s+1)$. The I-V characteristics can be described from an engineering analytical model of the PV array. Because the changing rate of the filtering capacitance voltage u_{Cf} is very small in steady-state operation, the current i_{Cf} of the filtering capacitor branch is negligibly small and i_{Lf} is almost equal to i_o. Thus, i_{Lf} replaces i_o for use as the feed current in the actual control system. The modeling and controller parameter design of the PV simulator are carried out mainly based on the inner-current loop.

According to the working principle and the input-output relationship of the PPF circuit, when S_1 (or S_2) is on, the relationship between the primary and secondary is:

$$\begin{cases} i_{in}=ni_{Lf} \\ u_F=nU_{in} \end{cases} \tag{5}$$

where i_{in}, i_{Lf} and u_F correspond to the instantaneous value of input current, the filtering inductor current and the pulse voltage rectified by the rectifying diodes, respectively.

When S_1 and S_2 are both off, the relationship is:

$$\begin{cases} i_{in}=ni_{Lf} \\ u_F=0 \end{cases} \tag{6}$$

By the above relationship and Kirchhoff's voltage and current laws, considering the effect of the inductance parasitic resistor R_f, the state-variable equations of the PPF circuit with S_1 (or S_2) being on are:

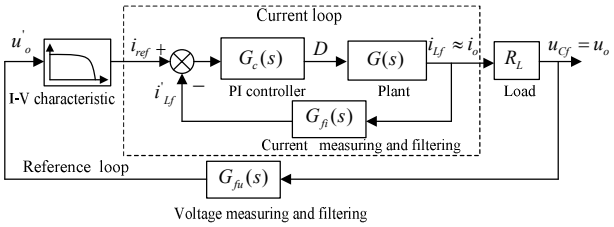

Fig. 5. Control block diagram of the digital PV simulator.

$$\begin{cases} L_f\dfrac{di_{Lf}}{dt}+\dfrac{T_{on}}{T_s}\cdot i_{Lf}R_f=u_F-\dfrac{T_{on}}{T_s}\cdot u_{Cf} \\ C_f\dfrac{du_{Cf}}{dt}+\dfrac{T_{on}}{T_s}\cdot\dfrac{u_{Cf}}{R_L}=\dfrac{T_{on}}{T_s}\cdot i_{Lf} \\ u_F=\dfrac{T_{on}}{T_s}\cdot nU_{in} \end{cases} \tag{7}$$

where $T_{on}=t_{0\text{-}2}$ or $T_{on}=t_{4\text{-}6}$, $t_{0\text{-}2}$ is the duration from t_0 to t_2 for each switch cycle, and $t_{4\text{-}6}$ is the duration from t_4 to t_6 for each switch cycle. The defining methods for the following similar variable are similar to $t_{0\text{-}2}$ and $t_{4\text{-}6}$.

Similarly, the state-variable equations of the PPF circuit when S_1 and S_2 are both off are:

$$\begin{cases} L_f\dfrac{di_{Lf}}{dt}+\dfrac{T_{off}}{T_s}\cdot i_{Lf}R_f=u_F-\dfrac{T_{off}}{T_s}\cdot u_{Cf} \\ C_f\dfrac{du_{Cf}}{dt}+\dfrac{T_{off}}{T_s}\cdot\dfrac{u_{Cf}}{R_L}=\dfrac{T_{off}}{T_s}\cdot i_{Lf} \\ u_F=0 \end{cases} \tag{8}$$

where $T_{off}=t_{2\text{-}4}$ or $T_{off}=t_{6\text{-}8}$.

Combining the above two switch statuses and according to the working mechanism of the simulator, the state space averaging equations of the PPF circuit in a switch time period are:

$$\begin{cases} L_f\dfrac{di_{Lf}}{dt}+\dfrac{2\left(T_{on}+T_{off}\right)}{T_s}\cdot i_{Lf}R_f=u_F-\dfrac{2\left(T_{on}+T_{off}\right)}{T_s}\cdot u_{Cf} \\ C_f\dfrac{du_{Cf}}{dt}+\dfrac{2\left(T_{on}+T_{off}\right)}{T_s}\cdot\dfrac{u_{Cf}}{R_L}=\dfrac{2\left(T_{on}+T_{off}\right)}{T_s}\cdot i_{Lf} \\ u_F=\dfrac{2T_{on}}{T_s}\cdot nU_{in} \end{cases} \tag{9}$$

Due to $T_{on}+T_{off}=T_s/2$, $D=2T_{on}/T_s$, the above equations can be rewritten in state space expression as:

$$\begin{cases} \begin{bmatrix} \dot{i}_{Lf} \\ \dot{u}_{Cf} \end{bmatrix}=\begin{bmatrix} -\dfrac{R_f}{L_f} & -\dfrac{1}{L_f} \\ \dfrac{1}{C_f} & -\dfrac{1}{R_LC_f} \end{bmatrix}\begin{bmatrix} i_{Lf} \\ u_{Cf} \end{bmatrix}+\begin{bmatrix} \dfrac{nU_{in}}{L_f} \\ 0 \end{bmatrix}D \\ i_{Lf}=\begin{bmatrix} 1 & 0 \end{bmatrix}\begin{bmatrix} i_{Lf} & u_{Cf} \end{bmatrix}^T \end{cases} \tag{10}$$

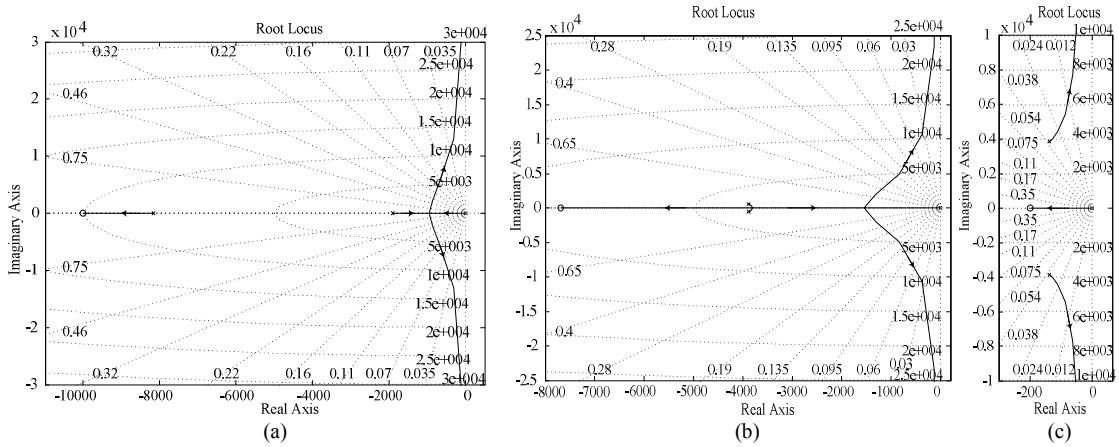

Fig. 6. Root loci of the current loop with k_i as variable((a) R_L=1Ω, (b) R_L=1.3Ω, and (c) R_L=50Ω).

Assuming that the initial conditions are zero, the transfer function of the duty ratio to the filtering inductor current by Laplace transforms of equation (10) can be obtained as:

$$G(s)=\frac{i_{Lf}(s)}{D(s)}=\begin{bmatrix}1 & 0\end{bmatrix}\begin{bmatrix}s+\frac{R_f}{L_f} & \frac{1}{L_f}\\ -\frac{1}{C_f} & s+\frac{1}{R_L C_f}\end{bmatrix}^{-1}\begin{bmatrix}\frac{nU_{in}}{L_f}\\ 0\end{bmatrix} \tag{11}$$

$$=\frac{nU_{in}}{L_f}\cdot\frac{s+\frac{1}{R_L C_f}}{s^2+\left(\frac{1}{R_L C_f}+\frac{R_f}{L_f}\right)s+\frac{R_L+R_f}{R_L L_f C_f}}$$

V. Controller Parameter Design of the Digital PV Simulator

A. Ideas of the Controller Parameter Design

The open loop transfer function of the current loop is:

$$G_{ok}(s)=G_c(s)G(s)G_{fi}(s)=\frac{k_p s+k_i}{s}\cdot\frac{nU_{in}}{L_f}\cdot \tag{12}$$

$$\frac{s+\frac{1}{R_L C_f}}{s^2+\left(\frac{1}{R_L C_f}+\frac{R_f}{L_f}\right)s+\frac{R_L+R_f}{R_L L_f C_f}}\cdot\frac{1}{T_{f1}s+1}$$

There are two parameters (k_p and k_i) that need to be determined in equation (12). k_p and k_i are usually designed to match with the transfer function $G(s)$. However, $G(s)$ varies with R_L, and R_L varies with the operating point and has a wide variation range. As a result, together with the high dimension of $G_{ok}(s)$, it is very difficult to determine the two controller parameters. If the pole of $G_{fi}(s)$ is cancelled by the zero of the PI controller, namely, $k_p/k_i=T_{fl}$, the design difficulty will be reduced to a certain extent. However, k_i remains difficult to determine due to the uncertainty of R_L.

Under the condition of $k_p/k_i=T_{fl}$, the performances of the root loci with k_i and R_L as variables are analyzed for designing the controller parameters. On the basis of the analytical method, several sets of PI controller parameters matched with different R_L are designed. In order to match the controller parameters with R_L, a fuzzy PI controller based on the Takagi-Sugeno fuzzy model is applied to self-adaptively regulate the controller parameters so as to satisfy the control demands as the operating point changes.

B. Performance Analysis of the Root Loci with k_i

The open loop transfer function of the current loop with k_i as a variable is:

$$G_{ok}(s)=G_c(s)G(s)G_{fi}(s)=\frac{k_i\cdot\frac{nU_{in}}{L_f}\cdot\left(s+\frac{1}{R_L C_f}\right)}{s^3+\left(\frac{1}{R_L C_f}+\frac{R_f}{L_f}\right)s^2+\frac{R_L+R_f}{R_L L_f C_f}s} \tag{13}$$

The root loci of the current loop with k_i as a variable for different values of R_L are a family of curves. It is found by analyzing the root loci that the root loci show three different types of motion curves with R_L=1.287Ω and R_L=1.403Ω as cut-off points. The typical root loci are shown in Fig. 6. It can be seen from the figure that the system is always stable no matter how R_L changes. However, the locations of the zeros and poles vary with R_L. For different locations of the zeros and poles, the performances of the current loop show large differences. At a given R_L, different closed-loop poles have different values of k_i and performance indexes, such as the damping ratio ζ and the overshot. It is obvious that the value of k_i determines the location of the closed-loop poles and the performances of the system.

C. Performance Analysis of the Root Loci with R_L

According to the characteristic equations of the closed current loop system, its open loop transfer function with R_L as a variable is rewritten as:

$$G_{ok}^{'}(s)=\frac{R_L\left[s^3+\frac{R_f}{L_f}s^2+\left(\frac{1}{L_fC_f}+\frac{k_inU_{in}}{L_f}\right)s\right]}{\frac{1}{C_f}s^2+\frac{R_f}{L_fC_f}s+\frac{k_inU_{in}}{L_fC_f}} \quad (14)$$

The root loci of the current loop with R_L as a variable for different values of k_i are also a family of curves. Although the locations of the zeros and poles change with k_i, the form of the root loci is basically the same. Typical root loci are shown in Fig. 7.

It can be seen from the figure that the system is always stable no matter how k_i changes. When k_i kept constant, different values of R_L have different performance indexes. Apparently, R_L is also a key factor to influence the system's performances.

D. Design of Controller Parameters

From the analysis presented above, it can be seen that only suitable values of k_i matched with R_L can satisfy the performance requirements of the system because R_L varies with the operating point.

For this purpose, by combining the time domain performance indexes of the equivalent 2-order system with the output characteristics of the PV array, typical operating points of the segmented operating ranges are selected to determine the closed-loop dominant poles and the corresponding k_i based on the root loci analysis. The closed-loop dominant poles are selected close to an imaginary axis and the absolute values of the real parts for the other close-loop poles and zeros are three times more than those of the closed-loop dominant poles. Once the closed-loop dominant poles are decided, the corresponding values of k_i can be calculated. For the given T_{f1}=0.01s, the value of k_p can be obtained according to the relationship $k_p/k_i=T_{f1}$. The PI controller parameters of the typical operating points in each of the segmented operating ranges are listed in Table I of the Appendix.

E. Self-adaptive Regulation of the Controller Parameters

It can be seen from the above analysis that the controller parameters must be regulated timely and appropriately according to R_L in order to obtain satisfactory dynamic and stationary performances. For these reasons, a fuzzy PI controller based on the Takagi-Sugeno fuzzy model is applied to regulate the controller parameters according to the change of the operating point of the PV simulator. The structure of the fuzzy PI controller is shown in Fig. 8.

In this paper, R_L is selected as the reference factor of the input variable, the input space is divided into four fuzzy subspaces based on the above design results of the controller parameter and every fuzzy subspace corresponds to the linear PI controller designed above. The models of the linear PI controllers are joined together smoothly by membership functions. With overlapping among the other inference rules,

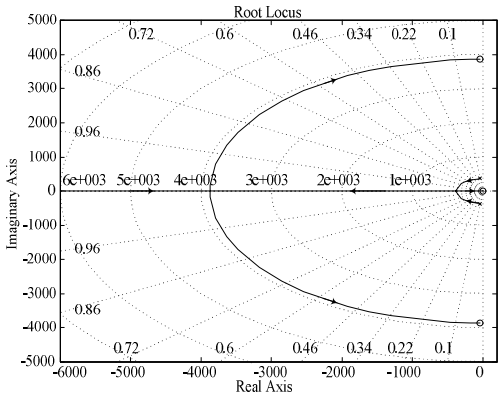

Fig. 7. Root loci of the current loop with R_L as variable.

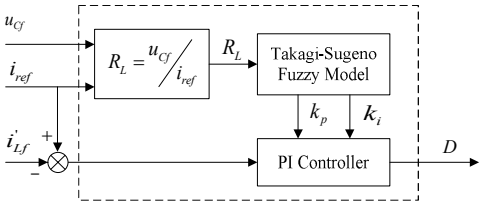

Fig. 8. Structure of fuzzy PI controller.

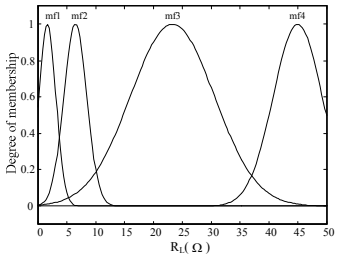

Fig. 9. Membership function of R_L.

the Takagi-Sugeno fuzzy model achieves the nonlinear global mapping and makes the PI controller parameters of each rule have a different weighting factor. Therefore, with the fuzzy inference of the Takagi-Sugeno fuzzy model, the PI controller parameters can self-adaptively regulate according to the change of the operating point and R_L. The value of R_c^i of the Takagi-Sugeno fuzzy model's fuzzy implication relationship has the following form [20]:

if R_L is A^i then $k_p=k_p^i$, $k_i=k_i^i$, $i=1, 2, \ldots, m$

where, i is the i-th rule; m is the number of fuzzy subspaces, m=4; A^i is the fuzzy subsets of the i-th rule; and k_p^i and k_i^i are the outputs of the i-th rule.

The total output of the fuzzy implication relation is given by:

$$k_p=\frac{\sum_{i=1}^{4}\mu_{A^i}(R_L)k_p^i}{\sum_{i=1}^{4}\mu_{A^i}(R_L)} \quad , \quad k_i=\frac{\sum_{i=1}^{4}\mu_{A^i}(R_L)k_i^i}{\sum_{i=1}^{4}\mu_{A^i}(R_L)} \quad (15)$$

where, $\mu_{A^i}(R_L)$ is the membership function of R_L and the application degree of the i-th rule and is decided by the membership degree for all of the input subsets in the rule.

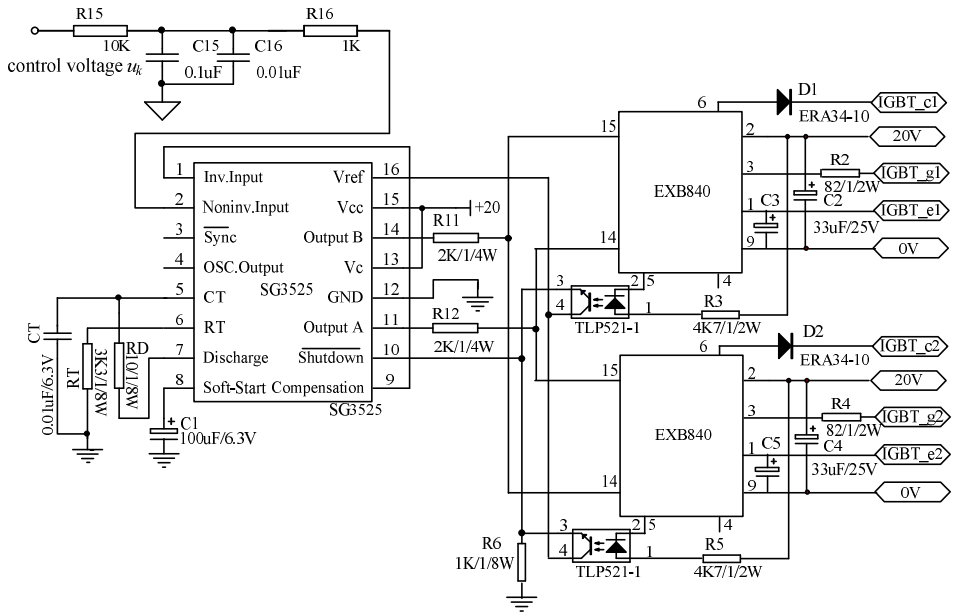

Fig. 10. Diagram of PWM signal generation, driving and isolating circuit.

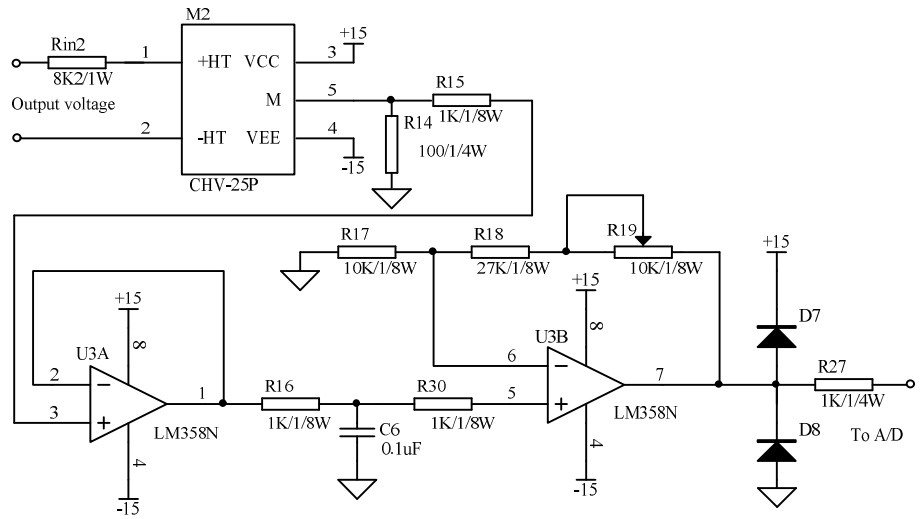

Fig. 11. Diagram of signal measuring and conditioning circuit.

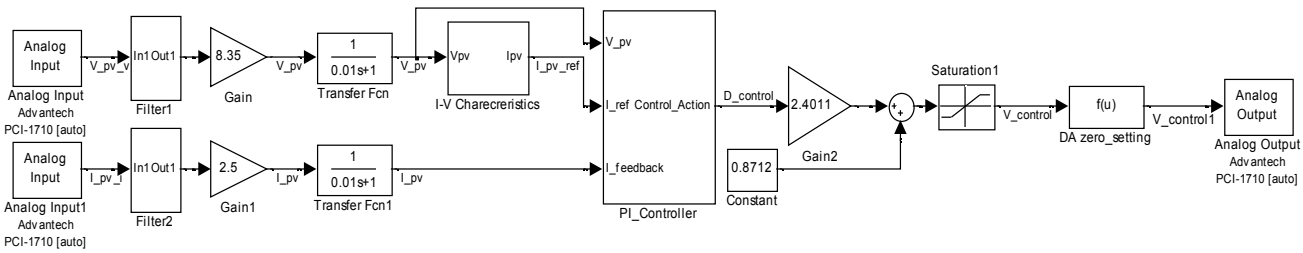

Fig. 12. Block diagram of real-time configuration and control program for digital PV simulator.

The membership function of R_L is the Gaussian type and it is shown in Fig. 9.

VI. Hardware and Software Design of the Digital PV Simulator

A. Push-Pull Forward Circuit

The design parameters of the PV simulator are shown in Table II of the Appendix. According to the above design requirements, the duty ratio of the PPF circuit and the turns ratio of the secondary to the primary are confirmed firstly.

Considered the extreme case where the maximum output voltage prescribed by the design indexes can be obtained under the minimum input voltage and the effective duty ratio is increased as much as possible in order to decrease the turns ratio of the secondary to the primary, the turns ratio of the secondary to the primary can be calculated by:

$$n = \frac{U_{o\max}}{D_{\max} U_{in\min}} = \frac{80}{0.9 \times 68} = 1.31$$

where D_{max} is the maximum duty ratio of the PPF circuit, D_{max}=0.9.

The other parameters of the high-frequency transformer are calculated by using the Area Product method. According to the working mechanism of the PPF circuit and considered a certain safety margin, 1MBH60D-100 IGBT modules and MUR3040PT diodes are selected as the power switches and output rectifying diodes, respectively.

According to the working mechanism of the PPF circuit, the averaging voltage of the clamping capacitor is equal to U_{in}. Due to the finite value of the clamping capacitor, there is a certain pulsating quantity of voltage Δu_{cb}, and it can be expressed as:

$$\Delta u_{cb} = \frac{I_a \Delta t_{3-4}}{C_b} \approx \frac{nD(1-D) I_o T_s}{2C_b} \tag{16}$$

Based on the estimation of the above formula and experimental research, a $10\mu F$ high-frequency non-inductive capacitor is selected as the clamping capacitor.

The key parameters of the PPF circuit are listed in Table III of the Appendix.

B. PWM Signal Generation, Driving and Isolating Circuit

In the PV simulator, a SG3525 is adopted as the pulse width modulation chip to generate two push-pull PWM signals according to the input control voltage. The two PWM signals generated by the SG3525 are amplified by two EXB840 modules to drive the power switches. The output signal of the EXB840's pin5 is sent to pin10 of the SG3525 by photocoupler so as to shut down the PWM signals for protecting the power switches when an overcurrent occurs. In order to prevent the power switches from turning on simultaneously, the two PWM signals are interlocked in the driving circuit so as to enhance the reliability of the system. A diagram of the PWM signal generation, driving and isolating circuit is shown in Fig.10.

C. Signal Measuring and Conditioning Circuit

The output voltage and inductor current are measured and converted into 0~2.5V voltage signals by Hall sensors. The signals are converted into 0~10V voltage signals by a signal conditioning circuit and then sent into a data acquisition card for A/D conversion. Taking the voltage measuring as an example, a diagram of the signal measuring and conditioning circuit is shown in Fig. 11.

D. Control and I/O Interface

The control and I/O interface of the PV simulator, which consists of a personal computer and a PCI1710 multifunction data acquisition card, can conveniently achieve the data acquisition and configuration of the control algorithm and interface by the abundant software resources of the computer.

E. Control Software Design

The modules of the Real-Time Windows Target are loaded to become a seamless integration of the Simulink environment and the external equipment under the external mode of Simulink, which can make Simulink become a real-time configuration development environment and a graphical control platform. In order to construct and adjust the models and parameters of the PV array, sunshine intensity, PV array's temperature and controller conveniently and to improve the software development efficiency and reliability, the control software of the PV simulator is designed and developed based on this configuration environment and control platform.

A diagram of the real-time configuration and control program for the PV simulator is shown in Fig.12. To increase the readability of the program, models of the I-V characteristics and the PI controller are both encapsulated into subsystems. Sampled-data control in equal intervals of time is adopted in the system and its sampling period is 1ms.

In order to solve the PV model conveniently, the engineering analytical model of the PV array, which can accurately describe the output characteristics of the PV array with only several electrical parameters under the standard test conditions provided by the manufactures and is convenient for engineering applications, is adopted to build the I-V characteristics subsystem in the MATLAB/Simulink environment. The engineering analytical model of the PV array can be expressed as [21]:

$$I_{PV} = I_{SC}(1 - C_1(e^{\frac{V_{PV} - DV}{C_2 V_{OC}}} - 1)) + DI \tag{17}$$

where:

$$C_1 = (1 - \frac{I_m}{I_{SC}}) e^{-\frac{V_m}{C_2 V_{OC}}}, \quad C_2 = (\frac{V_m}{V_{OC}} - 1) / \ln(1 - \frac{I_m}{I_{SC}}),$$

$$DV = -\beta \cdot DT - R_s . DI, \quad DI = \alpha \frac{Q}{Q_{ref}} \cdot DT + (\frac{Q}{Q_{ref}} - 1) \cdot I_{SC},$$

$DT = T - T_{ref}$, V_{OC} is the open-circuit voltage, I_{SC} is the short-circuit current, V_m is the optimum operating voltage and I_m is the optimum operating current, which gives the maximum power at that time. R_s is the series internal resistor, Q and Q_{ref} are actual sunshine intensity and the reference sunshine intensity of $1000 W/m^2$, respectively. T and T_{ref} are the actual module temperature and the reference temperature of 25 ℃, respectively. α and β are the current and voltage temperature coefficients under the reference sunshine intensity, respectively.

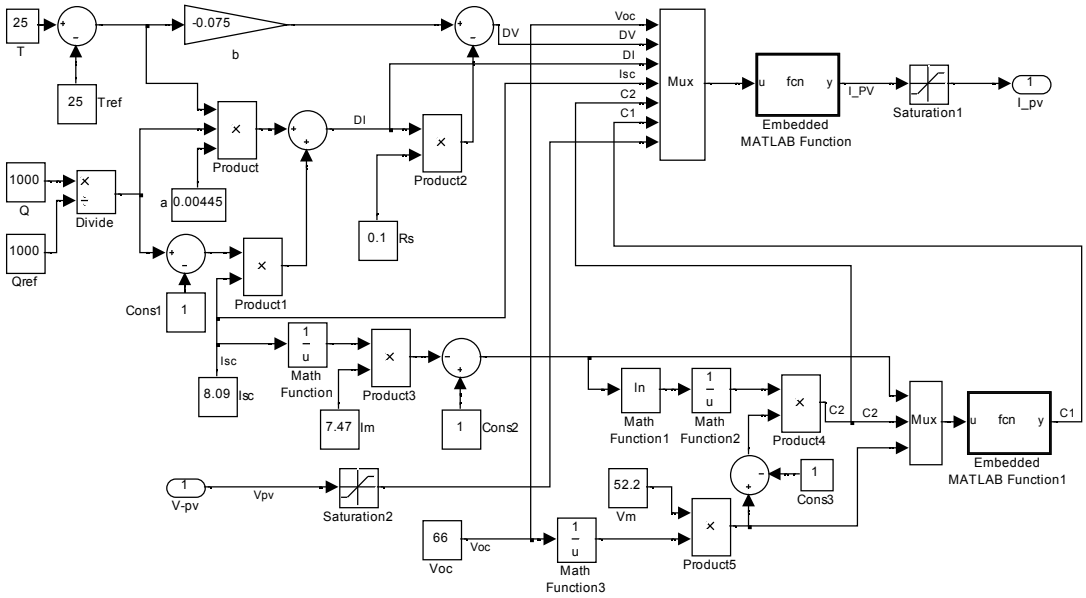

Fig. 13. Subsystem of I-V characteristics.

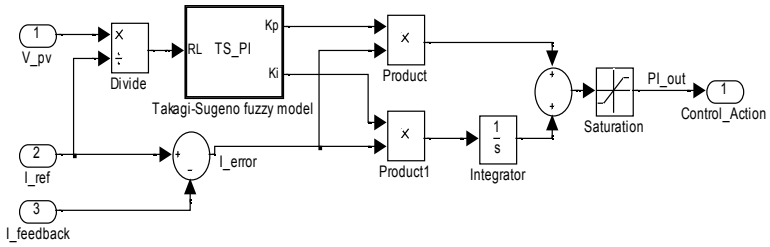

Fig. 14. Subsystem of fuzzy PI controller.

A diagram of the I-V characteristic subsystem is shown in Fig.13. It can be seen from the diagram that the models and parameters of the sunshine intensity, the PV array's temperature, etc. can be built and adjusted conveniently.

A diagram of the fuzzy PI controller subsystem is shown in Fig.14. In order to ensure real time control, the Takagi-Sugeno fuzzy model is realized with the Embedded MATLAB Function block of Simulink in the subsystem. The block can achieve complicated function flexibility with the MATLAB programming language and it can execute simulations and generate code for a Real-time Workshop target.

VII. EXPERIMENT RESULTS AND ANALYSIS

A. System Implementation

Based on the principle of modular hardware and configurable software, the functional modules of the PV simulator's hardware which consists of the PPF circuit, the PWM signal generation, the driving and isolating circuit, the measuring and signal conditioning circuit, the control and I/O interface, and so on, are all implemented and tested. After the module level test, all of the functional modules are connected with software to form a complete system and then tested in a whole system. In this paper, a DC programmable electronic load of IT8516C by ITECH is adopted to simulate the load characteristics. The whole system is shown in Fig.15, and the parameters of the PV array used to verify the performance of the PV simulator are listed in Table IV of the Appendix.

B. Steady-state Experiment

In the experiment, the load mutation test is done to verify the steady-state performances of the different operating points. The typical waveforms of the output voltage and filtering inductor current are shown in Fig.16. In the test, R_L is changed suddenly from 20Ω to 5Ω and then changed suddenly from 5Ω to 20Ω after remaining a 5Ω for some time. The experimental waveforms indicate that the ripples of the voltage and current are both very small and that the system can work steadily at the operating point corresponding with R_L. The PV simulator has a fast dynamic response and a high steady-state accuracy.

Based on the above results, the static output characteristics

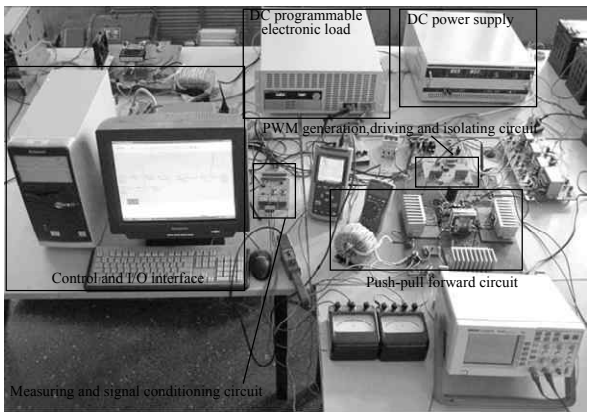

Fig. 15. Experimental setup of PV simulator.

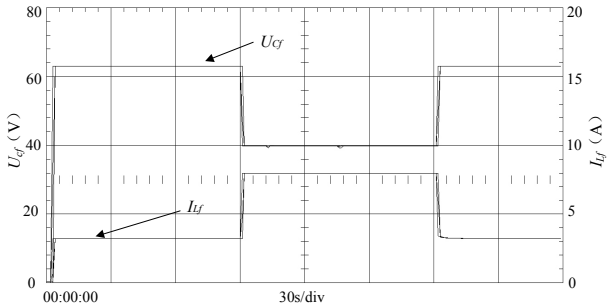

Fig. 16. Waveforms of output voltage and filtering inductor current.

of the PV simulator are simulated under 25℃ and different sunshine intensities as well as 1000W/m^2 sunshine intensity and different temperatures. Due to limitations on the length of this paper, only the static output characteristics under 25℃ and different sunshine intensities are given. The experimental results are shown in Fig.17.

The steady-state experimental results show that the output voltage and current of the PV simulator have a wide adjusting range, and that its current-voltage characteristics and power-voltage characteristics comply well with the theoretical output characteristics.

C. Dynamic Experiment

Due to variations of the operating point of the PV simulator with a load, the test of the power variation of the PV simulator with the sunshine intensity changed under natural conditions is done to verify the dynamic characteristic of the PV simulator. In the test, the sunshine intensity change under natural conditions is simulated by a combination of the positive and negative ramp function, and the other models. A DC programmable electronic load is selected in the constant-voltage mode to maintain a constant output voltage of the PV simulator so as to measure its output power. The curves of the sunshine intensity change and the output power for the PV simulator are shown in Fig. 18. The test result shows that the power of the PV simulator varies linearly with

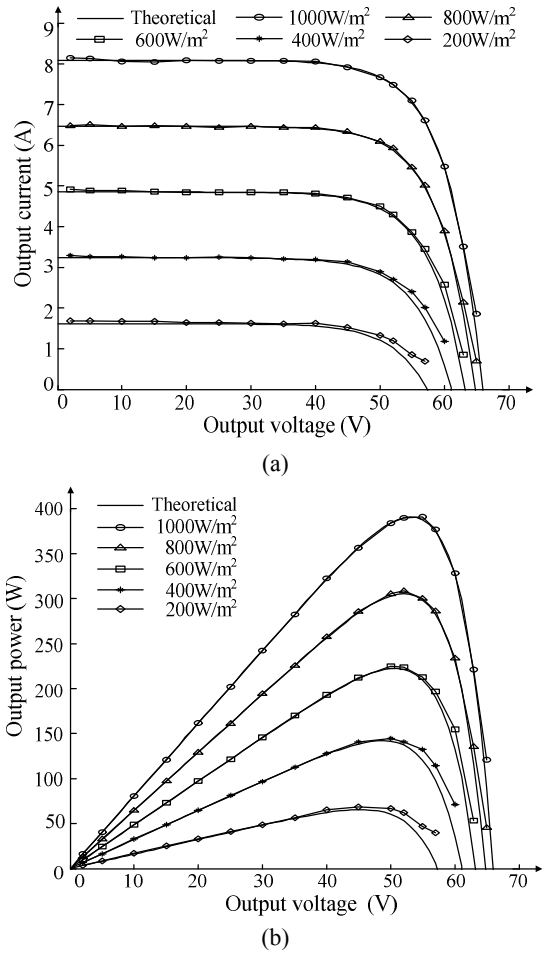

Fig. 17. Static output characteristics of PV simulator under 25℃ and different sunshine intensities ((a) Current-voltage characteristics and (b) Power-voltage characteristics).

the sunshine intensity change and it has a good dynamic response.

D. System Efficiency

The PV simulator's efficiency as a function of different output voltages under 1000W/m^2 sunshine intensity is measured. The efficiency curve is shown in Fig. 19. The efficiency curve shows that the PV simulator has a high working efficiency within a wide operating range and that it can satisfy the design requirements.

VIII. CONCLUSIONS

In this paper, the hardware of a digital PV simulator is designed and implemented based on the principle of modular hardware. The control structure of the system is based on a PC and a multifunction data acquisition card. A PPF circuit is adopted as the main circuit of the PV simulator to restrain the magnetic biasing of the core for the DC-DC converter and to reduce the spike of the turn-off voltage across every switch. Based on an analysis of the operating mode and the

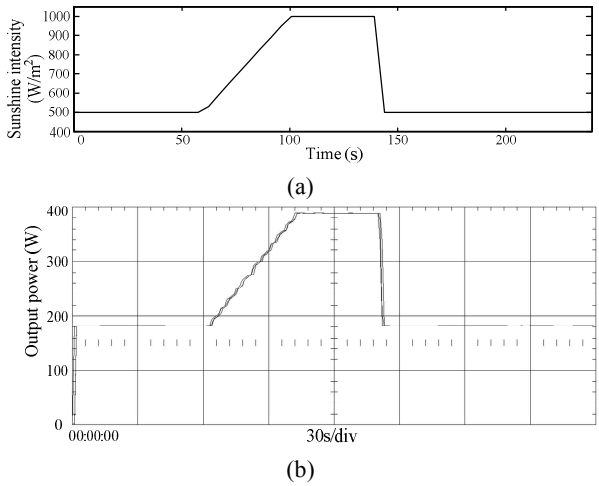

Fig. 18. Dynamic output characteristics of PV simulator ((a) curve of sunshine intensity change and (b) curve of output power of PV simulator).

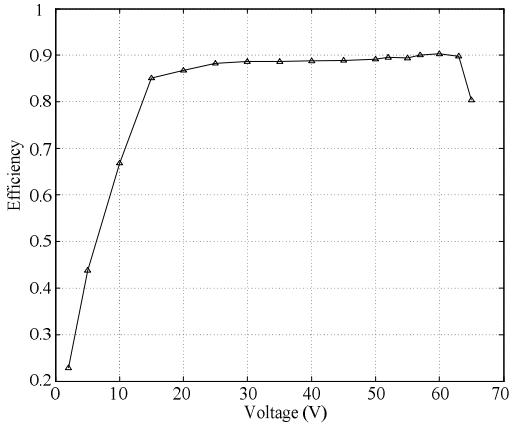

Fig. 19. Efficiency curve of the PV simulator in 1000W/m^2 sunshine intensity.

input-output relationship of the PPF circuit, mathematic models of the PPF circuit and PV simulator are built by the state-space averaging method. Aiming at the problem where the load resistance R_L changing with the operating point of the PV simulator leads to the difficult controller parameter design, the inertial element of the equivalent transfer function of current measuring, conditioning and filtering is cancelled by the pole-zero cancellation technique so as to reduce the design difficulty of the controller parameters. Then the controller parameters are systematically designed based on the performance analysis of the root loci of the closed current loop with k_i and R_L as variables. In order to match the controller parameters with R_L, a fuzzy PI controller based on the Takagi-Sugeno fuzzy model is applied to self-adaptively regulate the controller parameters.

The real-time configuration and the control program for the digital PV simulator are developed in the real-time environment of Matlab/Simulink which loads the modules of the Real-Time Windows Target and works under the external mode of Simulink so that the models and parameters of the system can be adjusted conveniently and the system can run in real-time. Lastly, the stationary and dynamic performances of the PV simulator are tested by experiments. The experimental results show that when the controller parameters designed in this paper according to the state-space averaging model are applied to the PV simulator, satisfactory dynamic and stationary performances are obtained. This makes it have the merits of a wide effective working range, a high steady-state accuracy and good dynamic performances. Therefore, it can be seen that the modeling and controller parameter design of the digital PV simulator based on the PPF circuit proposed in this paper is correct and reasonable. It also has a significant reference value for the modeling and controller parameter design of many other types of PV simulators and converters.

APPENDIX

TABLE I
PI PARAMETERS OF TYPICAL OPERATING POINTS

R_L	PI controller parameters	
	k_p	k_i
R_L<2	0.104	10.4
2≤ R_L<10	0.002	0.2
10≤R_L<40	0.01	1
R_L≥40	0.05	5

TABLE II
PARAMETER VALUES OF PV SIMULATOR

Parameter name	Value
U_{in}(V)	68-92
U_o(V)	0-80
P_o(W)	500
f_s(kHz)	20
η	>0.8

TABLE III
PARAMETER VALUES OF PPF CIRCUIT

Parameter name	Value
n	1.31
C_{in} (μF)	1000
C_b (μF)	10
L_f (mH)	0.675
C_f (μF)	100

TABLE IV
PARAMETER VALUES OF PV ARRAY

Parameter name	Value
V_{oc}(V)	66
I_{sc}(A)	8.09
V_m (V)	52.2
I_m(A)	7.47
P_m(Wp)	390
T(℃)	-40-85

REFERENCES

[1] E. M. Ahmed and M. Shoyama, "Scaling Factor design based variable step size incremental resistance maximum power point tracking for PV systems," *Journal of Power Electronics*, Vol. 12, No. 1, pp. 164-171, Jan. 2012.

[2] S. Thangaprakash, "Unified MPPT control strategy for z-source inverter based photovoltaic power conversion systems," *Journal of Power Electronics*, Vol. 12, No. 1, pp. 172-180, Jan. 2012.

[3] D.-H. Jang and S.-K. Han, "Low cost high power density photovoltaic power conditioning system with an energy storage system," *Journal of Power Electronics*, Vol. 12, No. 3, pp. 487-494, May 2010.

[4] S.-K. Ji, D.-H. Jang, and S.-S. Hong, "Analog control algorithm for maximum power trackers employed in photovoltaic applications," *Journal of Power Electronics*, Vol. 12, No. 3, pp. 503-508, May 2012.

[5] S. Lee, J.-E. Kim, and H. J. Cha, "Design and implementation of photovoltaic power conditioning system using a current-based maximum power point tracking," *Journal of Electrical Engineering & Technology*, Vol. 5, No. 4, pp. 606-613, Nov. 2010.

[6] Y. L. Shen, "A photovoltaic array simulator," *Acta Energiae Solaris Sinica*, Vol. 18, No. 4, pp. 448-451, Oct. 1997. (in Chinese)

[7] H. Nagayoshi, "I-V curve simulation by multi-module simulator using I-V magnifier circuit," *Solar Energy Materials & Solar Cells*, Vol. 82, No. 1-2, pp. 159-167, May 2004.

[8] Q. Li, Y. D. Li, K. Wang, J. Y. Rao, and Z. Y. Shen, "Design and development of solar array simulator," *Electric Drive*, Vol. 38, No. 5, pp. 8-10, May 2008. (in Chinese)

[9] L. Bun, B. Raison, G. Rostaing, S. Bacha, A. Rumeau, and A. Labonne, "Development of a real time photovoltaic simulator in normal and abnormal operations," in *Proc. IECON 2011*, pp. 867-872, 2011.

[10] A. C. Nanakos, and E. C. Tatakis, "Static and dynamic response of a photovoltaic characteristics simulator," in *Proc. EPE-PEMC 2008*, pp. 1827-1833, 2008.

[11] Y. Li, T. W. Lee, F. Z. Peng, and D. C Liu, "A hybrid control strategy for photovoltaic simulator," in *Proc. APEC 2009*, pp. 899-903, 2009.

[12] A. Koran, K. Sano, R.-Y. Kim, and J.-S. Lai, "Design of a photovoltaic simulator with a novel reference signal generator and two-stage LC output filter," *IEEE Trans. Power Electron.*, Vol. 25, No. 5, pp. 1331-1338, May 2010.

[13] A. Vijayakumari, A. T. Devarajan, and N. Devarajan, "Design and development of a model-based hardware simulator for photovoltaic array," *International Journal of Electrical Power and Energy Systems*, Vol. 43, No. 1, pp. 40-46, Dec. 2012.

[14] M. C. Di Piazza, M. Pucci, A. Ragusa, and G. Vitale, "Analytical versus neural real-time simulation of a photovoltaic generator based on a DC-DC converter," *IEEE Trans. Ind. Appl.*, Vol. 46, No. 6, pp. 2501-2510, Nov./Dec. 2010.

[15] F. S. Wang, J. Y. Wen, X. Zhang, and W. Zhao, "An investigation on digital photovoltaic array simulator," *Acta Energiae Solaris Sinica*, Vol. 33, No. 3, pp. 494-499, Mar. 2012. (in Chinese)

[16] J.-P. Lee, B.-D. Min, T.-J. Kim, J.-H. Kim, M.-H. Ryu, J.-W. Baek, D.-W. Yoo, and J.-Y. Yoo, "Development of a photovoltaic simulator with novel simulation method of photovoltaic characteristics," in *Proc. INTELEC 2009*, pp. 1-5, 2009.

[17] G. Martin-Segura, J. Lopez-Mestre, M. Teixido-Casas, and A. Sudria-Andreu, "Development of a photovoltaic array emulator system based on a full-bridge structure," in *Proc. EPQU 2007*, pp. 1-6, 2007.

[18] C. Z. Zhang, Q. F Chen, and J. Z. Zou, "Research on large capacity PV array simulator," *Acta Energiae Solaris Sinica*, Vol. 32, No. 10, pp. 1461-1465, Oct. 2011. (in Chinese)

[19] F. H. Zhang, H. H. Qin, H. Z. Wang, and Y. G Yan, "Freewheeling current in Push-Pull Forward converter," in *Conf. Rec. IEEE-PESC Annu. Meeting*, Vol. 1, pp. 353-358, 2003.

[20] J. K. Zhang, S. T. Wang, and Z. H Wang, "Nonlinear fuzzy PID control strategy for nonlinear plant with large inertia," in *Proc. WCICA 2010*, pp. 2537-2541, 2010.

[21] J. H. Su, S.-J. Yu, W. Zhao, M. Wu, Y. Shen, and H. He, "An investigation on engineering analytical model of silicon solar cells," *Acta Energiae Solaris Sinica*, Vol. 22, No. 4, pp. 409-412, Oct. 2001. (in Chinese)

Jike Zhang was born in Hohhot, China. He received his B.S. and M.S. degrees in Control Science and Engineering from the Inner Mongolia University of Technology, Hohhot, China, in 2000 and 2003, respectively. He is presently working toward his Ph.D. degree at the Inner Mongolia University of Technology. Since 2005, he has been a Lecturer in the Department of Automation, Inner Mongolia University of Technology. His current research interests include power electronics and control in renewable energy.

Shengtie Wang was born in Hohhot, China. He received his B.S. and M.S. degrees in Control Science and Engineering from the Chengdu University of Science and Technology, Chengdu, China, in 1985 and 1988, respectively. He received his Ph.D. degree in Electrical Engineering from the Huazhong University of Science and Technology, Wuhan, China, in 1999. Since 2000, he has been a Professor in the Department of Automation, Inner Mongolia University of Technology, Hohhot, China. From September to December of 2003, he was a Researcher at Mie University, Tsu, Japan, where he was engaged in research on the control of small wind turbines. From 2007 to 2008, he worked as a Visiting Scholar at the Norwegian University of Science and Technology (NTNU), Trondheim, Norway, where he was engaged in research on the control of large wind turbines. His current research interests include power electronics and control in renewable energy, intelligent control and applications.

Zhihe Wang was born in Baotou, China. He received his B.S. and M.S. degrees in Control Science and Engineering from Chongqing University, Chongqing, China, in 1985 and 1988, respectively. From 1991 to 1996, he worked for the Automation Research Institute, Inner Mongolia University of Technology, Hohhot, China, where he was engaged in research on electric drives, motion control, and power quality control. Since 2003, he has been a Professor in the Department of Automation, Inner Mongolia University of Technology. His current research interests include power electronics and converter control.

Lixin Tian was born in Baotou, China. He received his B.S. degree in Electronic Science and Technology from Inner Mongolia University, Hohhot, China, in 1989. From 1992 to 1996, he worked for the Automation Research Institute, Inner Mongolia University of Technology, Hohhot, China, where he was engaged in research on power electronics and power quality control. Since 2001, he has been a Assistant Professor in the Department of Electric Power, Inner Mongolia University of Technology. His current research interests include power electronics and energy conversion.